https://dx.doi.org/10.1016/j.tust.2020.103594

Evolutionary hybrid neural network approach to predict shield tunneling-induced ground settlements

Kun Zhang, PhD Candidate
Department of Civil Engineering, School of Naval Architecture, Ocean, and Civil Engineering, Shanghai Jiao Tong University, Shanghai 200240, China
Email: zhangjiaxuan@sjtu.edu.cn

Hai-Min Lyu, PhD, Research Associate
State Key Laboratory of Internet of Things for Smart City, University of Macau, Macau, China
Email: haiminlyu@um.edu.mo

Shui-Long Shen*, PhD, Professor
Department of Civil and Environmental Engineering, College of Engineering, Shantou University, and Key Laboratory of Intelligent Manufacturing Technology (Shantou University), Ministry of Education, China.
Shantou, Guangdong 515063, China
Email: shensl@stu.edu.cn
Phone and Fax: (86)754-8650-4551
ORCID: 0000-0002-5610-7988.

Annan Zhou, PhD, Associate Professor
Civil and Infrastructure Discipline, School of Engineering, Royal Melbourne Institute of Technology (RMIT), Victoria 3001, Australia;
Email: annan.zhou@rmit.edu.au
ORCID: 0000-0001-5209-5169

Zhen-Yu Yin, PhD, Associate Professor
Department of Civil and Environmental Engineering, The Hong Kong Polytechnic University, Hung Hom, Kowloon, Hong Kong.
Email: zhenyu.yin@polyu.edu.hk;

To be submitted to

Tunnelling and Underground Space Technology

June 23, 2020

Evolutionary hybrid neural network approach to predict shield tunneling-induced ground settlements

Kun Zhang, Hai-Min Lyu, Shui-Long Shen*, Annan Zhou, Zhen-Yu Yin

Abstract

This study proposes an artificial intelligence approach to predict ground settlement during shield tunneling via considering the interactions among multi-factors, e.g., geological conditions, construction parameters, construction sequences, and grouting volume and timing. The artificial intelligence approach employs a hybrid neural network model that incorporates a differential evolution algorithm into the artificial neural network (ANN). The differential evolution algorithm is used to determine the optimized architecture and hyperparameters of the ANN. The adaptive moment estimation (Adam) method is then employed to facilitate the training process of ANN. On the strength of Adam, the differential evolution algorithm is further enhanced to process a large number of ANN candidates without consuming massive computing resources. The proposed hybrid model is applied to a field case of ground settlements during shield tunneling in Guangzhou Metro Line No. 9. Geological conditions and shield operation parameters are first characterized and quantified by a feature extraction strategy, then input for the model. Results verifies the accuracy of prediction using the proposed hybrid model. Moreover, shield operation parameters with high influence on ground settlement are identified through a partial derivatives sensitivity analysis method, which can provide guidance for shield operation.

Keywords: Settlement prediction; Tunneling; Differential evolution algorithm; ANN; Sensitivity analysis.

1 Introduction

Shield tunneling is widely used for underground tunnel construction in various geological conditions such as soft deposits (Shen et al. 2009; Wu et al. 2019), weak rocks (Ren et al. 2018c), and mixed grounds with soft soils and rocks (Elbaz et al. 2018, 2020). Ground settlement associated with the shield tunneling is a common issue (Peck, 1969; Shen et al. 2010, 2016; Ren et al, 2018a, c), which may cause structural deformation and cracking, and potentially threaten the adjacent facilities (Giardina et al. 2013; Fu et al. 2014; Camós et al. 2015; Soga et al. 2017). Therefore, an improved understanding of ground response to tunnel excavation is essential for securing the tunnel construction and building environment safety, particularly considering an increasing demand for the underground transportation construction due to fast urbanization in recent years (Mair 2008; Fargnoli et al. 2015). A key challenge is then to clarify and quantify the nonlinear soil-shield interactions during excavation (Wongsaroj et al. 2013; Tan and Lu 2017, 2018).

Over the past 50 years, numerous approaches have been developed to model the tunneling-induced ground settlements (Chai et al. 2018). The most widely used approaches in engineering practice are empirical methods and numerical methods. Empirical method was firstly proposed by Peck (1969) who advocated using invert Gaussian distribution curve to predict tunneling-induced ground settlements profile. Then, some modified empirical formulae have been put forward (Mair 1996, Vorster et al. 2005). Although empirical methods are convenient, without considering the realistic incorporation of all the relevant spatial-temporal interactions occurring during tunneling, their application situation is limited (Meschke 2018). Numerical methods can model the complex tunneling processes by incorporating constitutive models for rocks/soils, complex boundary conditions and dynamic construction procedures (Ninić 2015; Lyu et

al. 2020a; Wu et al. 2020; Wu et al. 2020a, 2020b). However, geological parameters required for model development and calibration are not readily available, and uncertainties are inevitably embedded in model parameters. Thus, it is difficult to implement the numerical model in many cases (Wang et al. 2016; Liu et al., 2019; Atangana et al. 2020; Gao et al. 2020; Lyu et al. 2020b). Except for the empirical and numerical methods, machine learning methods have gradually emerged as promising approaches that can predict ground settlements with limited knowledge of the underlying physical parameters and the intermediate physical processes. Machine learning methods can find regularities hidden in historical data and then apply them to predict future scenarios (Sahoo et al. 2017; Chen et al. 2019b; Zhang 2019; Zhang et al. 2020). Many researchers have developed various machine learning models for geotechnical engineering, such as artificial neural network (ANN) (Kim et al. 2001; Suwansawat et al. 2006; Santos et al. 2008; Freitag et al. 2017; Chen et al. 2019a), genetic algorithm (Yin et al. 2017), support vector machine (Samui et al. 2008; Zhao et al. 2009), relevance vector machine (Wang et al. 2016), adaptive neuro fuzzy based inference system (Bouayad et al. 2017), decision tree (Dindarloo et al. 2015), random forest (Zhang et al. 2019), etc.

ANN is the most popular model among the aforementioned models due to its great potential in dealing with high nonlinear interactions between input and objective parameters. Generally, optimal architecture of ANN varies for different issues in many cases. Thus, it is necessary to make a sound design to fully explore the potential of ANN models conducted for the prediction of tunneling-induced ground settlements. Suwansawat et al. (2006) used trial-and-error way to determine the best number of hidden layers and neurons. Whereas, Kim et al. (2001) and Santos et al. (2008) determined the architecture of ANN directly. These studies only tested few or certain ANN models, thereby potentially restricting their applicability. Besides, the selection of

input parameters is also significant to the establishment of ANN models. Tunnel geometry, geological conditions and shield operation parameters are often considered as the input parameters (Suwansawat et al. 2006; Wang et al. 2016). However, most research works simply take account of the geological categories rather than the physical properties for geomaterials. Such a simplification may provide insufficient information on soil characteristics for ANN models. Another key issue when forming ANN predictive models is how to assess the relative importance of input parameters to the objective output (Kemp et al. 2007; Paliwal et al. 2011). Accurate knowledge of relative importance would be useful in guiding shield steering and monitoring. Common methods for identifying relative importance in ANN contain connection weight method, perturb method, profile method and partial derivatives method (Oña et al. 2014). The first method is only suitable for ANN with a single hidden layer while the latter three can be competent for ANN with multiple hidden layers.

The objective of this study is to predict tunneling-induced ground settlements by developing a novel ANN model enhanced by the differential evolutionary algorithm. First, a hybrid neural network model is developed to incorporate the differential evolutionary algorithm into the ANN. The proposed hybrid model is then employed to predict the ground settlements induced by shield tunneling. The relative importance of input parameters (especially the shield operation parameters) to ground settlement is identified by using the proposed hybrid model.

2 Brief review on ANN

Fig. 1 shows a typical ANN architecture, which consists of one input layer, one output layer, and one or more hidden layers in between. Each layer has several processing units, called neurons. In a fully connected ANN, two neurons in the adjacent layers have a connection, by which the input signals can flow from the input layer to the

output layer to generate processed data. The hidden layers are important because most of mathematical adjustment operations are performed within them. As shown in Fig.1, the neurons arranged in these layers executes two vital phases, namely (*i*) linear regression and (*ii*) activation, the aforementioned two phases can be written as

$$z_l^j = \sum_{i=1}^{n} w_l^{ji} a_{l-1}^i + b_l^j, \quad (j = 1, ..., m) \tag{1}$$

$$a_l^j = g\left(z_l^j\right) \tag{2}$$

where a_{l-1}^i is the output of the i^{th} neuron in the $(l\text{-}1)^{\text{th}}$ layer, w_l^{ji} is the connection weight between the j^{th} neuron in the l^{th} layer and the i^{th} neuron in the $(l\text{-}1)^{\text{th}}$ layer, b_l^j is the bias associated with the j^{th} neuron in the l^{th} layer, z_l^j is the linearized values corresponding to the j^{th} neuron in the l^{th} layer, n is the number of neurons in the $(l\text{-}1)^{\text{th}}$ layer, m is the number of neurons in the l^{th} layer, and $g()$ is the activation function. In this paper, the tanh function ranged between (-1, 1) is used as the activation function for all the layers.

Each neuron has different values of weights and biases that indicate the influences of input data. The initial weights are crucial to the performance of the ANN because of the multiplicative effect through layers. Glorot et al. (2010) suggested using the following normalized initialization method for the initial weights.

$$w_l \sim U\left[-\frac{\sqrt{6}}{\sqrt{n_{l-1}+n_l}}, \frac{\sqrt{6}}{\sqrt{n_{l-1}+n_l}}\right] \tag{3}$$

where $U[-v, v]$ is the uniform distribution in the interval $(-v, v)$ and n_l is the number of the neurons in the l^{th} layer.

Generally, the estimated values outputted through the network are different from the target values. In the training of an ANN model, the differences are usually called

"loss" or "cost". Given the proposed ANN architecture, the *log-cosh* loss function is adopted, which can be expressed in the following form.

$$L(\boldsymbol{w},b)=\frac{1}{M}\sum_{p=1}^{M}\log\left(\cosh\left(\hat{y}_p-y_p\right)\right) \tag{4}$$

where M is the size of sample, y_p and $\hat{y}_p$ are the target value and the predicted value for the p^{th} example, respectively. This loss is similar to the mean square error but is not easily subject to outliers. To prevent overfitting, "L^2 regularization" term is added to Eq. (4), then the modified $L(\boldsymbol{w},b)$ becomes:

$$\tilde{L}(\boldsymbol{w},b)=L(\boldsymbol{w},b)+\frac{\lambda}{2M}\boldsymbol{w}^T\boldsymbol{w}=L(\boldsymbol{w},b)+\frac{\lambda}{2M}\sum\left\|w_l^{ji}\right\|^2 \tag{5}$$

where λ is a hyperparameter that determines the level of regularization. This regularization strategy promotes generalizability of the neural network by driving the weights closer to the origin. Subsequently, the weights and biases can be updated as follows.

$$\begin{aligned} w_l^{ji}&=\left(1-\frac{\lambda\alpha}{M}\right)w_l^{ji}-\alpha\frac{\partial L}{\partial w_l^{ji}}\\ b_l^{j}&=b_l^{j}-\alpha\frac{\partial L}{\partial b_l^{j}} \end{aligned} \tag{6}$$

where α is the learning rate that controls the magnitude of parameter updates. By adjusting weights and biases in the opposite direction, the loss L gradually decreases epoch by epoch.

3 Proposed approach: hybrid neural network model

3.1 Algorithm with adaptive learning rates

Learning rate is a crucial parameter in training neural networks because of the significant influence on the model performance. On the other hand, the learning rate has long been regarded as one of the most difficult hyperparameters to set (Goodfellow et al. 2016). Recently, several incremental methods have been proposed to adapt the learning

rate automatically throughout the course of learning. Kingma et al. (2014) proposed an adaptive learning rate optimization algorithm (the 'Adam') that only demands first-order gradients with low memory requirement. This method combines the advantages of AdaGrad method (Duchi et al. 2011) and RMSProp method (Tieleman et al. 2012), which is regarded as being fairly robust to choose appropriate hyperparameters. Considering the prediction of ground settlements induced by shield tunneling using ANN requires a great deal of computing resources, this study employs the 'Adam' algorithm to accelerate backward propagation. The implementation of the 'Adam' algorithm is presented in Appendix (see Algorithm 1). Detailed introduction about Adam can be found in Kingma et al. (2014).

3.2 Differential evolution approach

Since there are no clear theories available to refer (Suwansawat et al. 2006), the architecture and the inherent hyperparameters of neural network in many research works are determined through trial-and-error method. Nevertheless, this method is less effective and prone to lead to suboptimal solutions. On the other hand, the design of a neural network is actually a kind of optimization problem. In view of this, this study employs differential evolution algorithm to determine the best neural network architecture (including the number of hidden layers and the number of neurons in a hidden layer) and hyperparameters (including epoch size and regularization parameter). Note that in this study, each hidden layer is set to have a same number of neurons.

Differential evolution algorithm proposed by Storn et al. (1997) is a simple yet powerful population-based optimizer over continuous space. The differential evolution algorithm has gradually gained more attention and has been widely used in diverse fields. The basic implementation of this algorithm is described as follows.

Initialize population. Differential evolution algorithm utilizes a certain amount of *D*-dimensional parameter vectors, i.e., individuals

$$\boldsymbol{x}_{i,g}\ ,\ \ i=1,2,...,N_P\ ,\ \ g=1,2,...,G \tag{7}$$

as a population for each generation *g*. N_P is the population size and *G* is the number of generations. The initial population should be uniformly distributed in the entire search space as much as possible. Let $\boldsymbol{X}_{\min}=\left\{x_{\min}^1,...,x_{\min}^D\right\}$ and $\boldsymbol{X}_{\max}=\left\{x_{\max}^1,...,x_{\max}^D\right\}$ be the prescribed minimum and maximum parameter bounds, respectively. Then the initial population can be expressed as below.

$$x_{i,0}^j=x_{\min}^j+rand\left(0,1\right)\cdot\left(x_{\max}^j-x_{\min}^j\right),\quad j=1,2,...,D \tag{8}$$

where $x_{i,0}^j$ is the j^{th} component of i^{th} individual in the initial generation, and *rand* (0, 1) represents a random value within the range (0, 1).

Mutation operation. Let $\boldsymbol{v}_{i,g}$ be the mutant vector. The following mutant vector generation strategy is selected to operate population mutation.

DE/rand/1: $$\boldsymbol{v}_{i,g}=\boldsymbol{x}_{r1,g}+F\left(\boldsymbol{x}_{r2,g}-\boldsymbol{x}_{r3,g}\right) \tag{9}$$

where "DE/rand/1" is a common mutant strategy used in differential evolution algorithm, r_1 , r_2 and $r_3\in\left\{1,2,...,N_P\right\}$ are mutually exclusive integers which are also different from *i*. *F* is a real and constant factor $\in$ [0, 2] for scaling the differential variation $\left(\boldsymbol{x}_{r2,g}-\boldsymbol{x}_{r3,g}\right)$.

Crossover operation. In the basic version, differential evolution algorithm uses the binomial (uniform) crossover. Let $\boldsymbol{u}_{i,g}$ be the trail vector which is given by

$$u_{i,g}^j=\begin{cases}v_{i,g}^j,\ \text{if}\ \left(\text{rand}(0,1)\le C_R\right)\ \text{or}\ \left(j=j_{rand}\right)\\ x_{i,g}^j,\ \text{otherwise}\end{cases} \tag{10}$$

where $u_{i,g}^j$ is the j^{th} component of $\boldsymbol{u}_{i,g}$, C_R is the crossover rate ($\in$ [0, 1]) that controls the fraction of individual component copied from the mutant vector, j_{rand} is a randomly selected integer in the range [1, D].

Selection operation. Let f denote the objective function acting on parameters of an individual. The selection follows the Greedy policy:

$$\boldsymbol{x}_{i,g+1} = \begin{cases} \boldsymbol{u}_{i,g}, & \text{if } f(\boldsymbol{u}_{i,g}) > f(\boldsymbol{x}_{i,g}) \\ \boldsymbol{x}_{i,g}, & \text{otherwise} \end{cases} \tag{11}$$

where $\boldsymbol{x}_{i,g+1}$ is the individual vector at the next generation.

In order to build the neural network prediction model, four variables, namely the number of hidden layers N_h, the number of neurons in a hidden layer N_n, epoch size E_s and regularization parameter λ, are denoted as the component of an individual $\boldsymbol{x}$. Therefore, the aim of employing the differential evolution algorithm is to find the optimal $\boldsymbol{x}$ for the neural network.

3.3 Sensitivity analysis

To quantify the importance of the various input parameters on the outputs within the neural network, the partial derivatives method (Dimopoulos et al. 1995) is employed in this study. Gevrey et al. (2003) compared seven different methods to determine the relative importance of input parameters and concluded that the partial derivatives method can produce the most stable results. The other advantage of this method is its ability in calculating relative importance of a neural network with multiple hidden layers.

The partial derivatives method calculates the first-order derivatives of the output parameter with respect to the input parameters and sums the derivatives across all the hidden layers. Based on the chain rule, we have

$$\begin{aligned} d_l^j &= \frac{\partial z_l^j}{\partial x_k} = \sum_{i=1}^{m} \frac{\partial z_l^j}{\partial z_{l-1}^i} \frac{\partial z_{l-1}^i}{\partial x_k} = \sum_{i=1}^{m} w_l^{ji} g'\left(z_{l-1}^i\right) \frac{\partial z_{l-1}^i}{\partial x_k} \\ &= \sum_{i=1}^{m} w_l^{ji} g'\left(z_{l-1}^i\right) d_{l-1}^i \end{aligned} \tag{12}$$

$$d_1^j = \frac{\partial z_1^j}{\partial x_k} = w_1^{jk} \tag{13}$$

$$s_k = \frac{\partial \hat{y}}{\partial x_k} = g'\left(z_L^1\right) d_L^1 \tag{14}$$

where d_l^j and s_k are the differential coefficients, and x_k is the k^{th} input parameter. Then, the relative importance of the k^{th} input parameter can be defined as below.

$$S_k = \sum_{p=1}^{M} \left(s_k^{(p)}\right)^2 \tag{15}$$

where M is the total number of observations.

The S (see equation (15)) provides a classification of the input parameters according to their contribution to the output parameter in an ANN model. The input parameter with the highest S value influences the output parameter most. The key parameters for the shield tunneling operation affecting the ground settlement significantly, can be identified by different S values.

3.4 Implementation of the hybrid model

The flowchart of the proposed evolutionary neural network model is shown in Fig. 2. The steps for the implementation of the proposed hybrid model for the shield tunneling-induced ground settlements prediction can be presented as follows.

Step 1: Analyzing geological conditions and collecting shield construction data, identifying the factors that potentially affect ground settlements and pre-processing the collected data (including parameter quantization and initialization).

Step 2: Applying the differential evolution algorithm to generate certain sets of neural network model parameters (N_h, N_n, E_s, and λ) at each iteration ("generation").

Step 3: Building the neural network models based on the parameters from **Step 2**.

Step 4: Training the developed models and comparing the predicted ground settlements with the measured ground settlements for each model in the current generation of differential evolution algorithm.

Step 5: Judging whether the best model in the current generation meets the desired

loss or whether the generation reaches the set value. If not, returning to **Step 2** and continuing the evolution process until the criterions are satisfied.

Step 6: Exporting the neural network with the best performance.

3.5 Application of the hybrid model

As shown in Fig. 3, the proposed hybrid model can be applied to a stage-wise design for shield machine steering. In the early stage of shield tunneling, owing to insufficient monitoring data available to implement the hybrid model, the empirical methods, analytical methods, and numerical methods can be adopted to provide initial guidance for shield machine operation. In the normal construction stage, the amount of monitoring data increases. Once the data is sufficient, the hybrid model can be activated to assist the shield tunneling operation. Meanwhile, the sensitivity analysis can be employed to identify the most influential operation parameters for shield tunneling. As the shield tunneling continues, new data will be generated continuously. These new data will enlarge the existing data set and consequently enhance the predictive performance of the proposed hybrid model.

4 Case study

4.1 Site and geological conditions

In this study, the relevant data during the construction of the tunnel between Maanshan Park Station and Liantang Station (M-L) are collected to evaluate the proposed approach. The M-L tunnel constitutes the middle section of Guangzhou Metro Line No. 9. It is subdivided into two main tunnel sections, i.e., the north tunnel section and the south tunnel section. The twin tunnels (the north line and the south line) are about 1.2 km in length, 6.0 m in outer diameter, and 5.4 m in inner diameter. The tunnel alignment passes through heavily crowded areas of Guangzhou city (Liu et al. 2018, 2019; Lyu et al. 2019; Ren et al. 2018b). Two earth pressure balanced (EPB) TBMs

were used to excavate the tunnel with a buried depth varying from 7.0 to 10.0 m. The geological profiles of the north and south tunnel subsections of M-L section are shown in Fig. 4.

Geological investigations indicate that different soil layers are not clearly stratified but often intersected, causing difficulties in establishing either an analytical or numerical model. For simplification, silty clay, sand, residual soil and highly weathered limestone are classified as the sand-clay soil in general in this study. Therefore, in the studied section, soils and rocks are divided into 3 layers, including the backfill, the sand-clay soil, and moderately weathered limestone. The tunnel was excavated mostly within the sand-clay layer but with few parts in the moderately weathered limestone. As shown in Fig. 4, karst caves have been detected and they are largely distributed in this site, which make the site difficult for tunnel construction. It has been widely acknowledged that engineering problems such as water inflow and shield head sinking occur with a high frequency when tunnels are excavated in a karst region (Cui et al. 2015; Elbaz et al. 2018). Therefore, most of these karst caves were treated by grouting cement to guarantee safe construction. To obtain the real-time feedbacks of ground response (like settlement) during the tunnel excavation, surface settlement markers were installed with approximately 5 m intervals along the tunnel alignment (see Fig. 4). By using these markers, the monitoring data were collected and subsequently stored in a database for establishing the prediction model.

4.2 Data analysis and pre-processing

The factors influencing ground settlements can be divided into three categories in general: (*i*) tunnel geometry, (*ii*) geological conditions, and (*iii*) operation parameters of shield machine. Given that the twin tunnels have a constant diameter and are excavated by the same type of EPB shield machine, the effects of tunnel geometry are neglected.

Thus, only geological conditions and shield operation parameters are considered in this example. Table 1 details all the parameters used as inputs to design the neural networks and some geological parameters and shield operation parameters in the EPB tunneling are visualized in Fig. 5.

The geological conditions include groundwater level (GL), thickness of backfill over tunnel crown (BCT), thickness of sand-soil over tunnel crown (SCT), thickness of weathered rock over tunnel crown (RCT), thickness of sand-soil under tunnel invert (SIT), thickness of rock under tunnel invert (RIT), height of karst cave (KH) and distance between karst cave and tunnel invert (KD). The soil thicknesses rather than detailed soil properties are considered in this study because quite a few indicators jointly characterize the soil that may result in complex computation. However, for certain soil, the settlement is approximately linear with the thickness of the soil as reflected in layer-wise summation method. The shield tunneling operation parameters considered in this study are selected based on previous research and on the particular site observations. The selected operation parameters include total thrust (T) to push the TBM during the excavation of each ring, cutter head torque (CT), penetration rate (V), tail void grouting pressure (GP), grouting volume (GV), face pressure (FP), tunneling deviation (TD), tail void (TV), karst cave treatment scheme (KTS). The 17 parameters mentioned above should be quantified in the hybrid model, and 16 of them can be determined directly from the recorded data except KTS. In this study, we set a dummy variable to represent KTS and stipulate that KTS =1 represents karst cave with treatment, KTS =0 represents karst cave without treatment and KTS =0.5 represents no karst caves detected.

Fig. 6 shows the excavation processes of the twin tunnels. The south tunnel was excavated on November 16, 2013, about one month earlier than the north tunnel. Then, the two tunnels were excavated almost parallelly until May 3, 2014 when most of the

cutting tools needed to be changed in the south tunnel. Fig. 7 plots the variation of six shield operation parameters in tunneling process of the south line. As can be seen in Fig. 7, the total thrust is between 4MN and 16MN, with an average value of 9.4MN. The variation of total thrust exhibits three undulating stages, which is close to the undulation of stratum. The cutter head torque varies in the range 1.0 - 3.0MN·m, with an average value of 1.8MN·m. Since the first 100 rings are in the trial excavation phase, the shield operator's unfamiliarity with the ground condition resulted in an obvious fluctuation of the torque. It can also be observed that the harder the soils at the cutting face, the larger the required torque of the cutter wheel. The variation of penetration rate is related to the soil type at the cutting face. When tunneling happens in rock or sand-rock formations, the penetration rate of shield machine is controlled below 40 mm/min. Besides, the face pressure varies in the range 100–300 kPa. Basically, the greater the variation in soil type at the cutting face, the greater the change in face pressure. Compared with other parameters, the variation of grouting pressure and grouting volume is relatively small, and most of the time they are kept at a constant value. From the above, it is seen that the complicated soil conditions in the M-L tunnel section lead to significantly changing shield operation parameters, implying that there is a strong interaction between the soils and the shield in the M-L tunnel section.

In order to explore key information from the soil-shield interaction for ground settlement prediction, 328 data samples are collected in this studied site including 176 on the north line and 152 on the south line. Among these samples, the maximum ground settlements above the tunnel centerline (see Fig. 8) are considered for the establishment of the proposed hybrid evolutionary model. Then, 270 data samples are randomly selected as training set while the remaining 58 samples are used as testing set. All the 17 input parameters mentioned before and the output ground settlement value in the training and testing set are normalized to the range of [-1, 1]. Normalization uses the

maximum and minimum values of the corresponding parameter in the whole data set, as expressed below.

$$x_i = 2 \times \frac{x_i - min(x)}{max(x) - min(x)} - 1 \tag{16}$$

where $min(x)$ and $max(x)$ are the minimum and maximum of a parameter, respectively. To evaluate the predicting capability of the proposed hybrid model, two evaluation criteria are employed in this paper (see Table 2).

4.3 Optimized neural network prediction model

Regarding the model design, the values of parameters applied to the differential evolution algorithm and the predefined range of parameters for determining neural network are listed in Table 3. The loss $\tilde{L}$ instead of evaluation criteria is used as objective function to guide the algorithm in the evolutionary process because *log-cosh* loss function is smooth and less susceptible to outliers than evaluation criteria. Indeed, the loss function and the mentioned criteria function are basically consistent in reflecting the decreasing trend of the difference between the predicted value and the measured value, ensuring the reliability of the obtained prediction model.

After performing an optimization using the differential evolution algorithm on the dataset, the neural network model with a high ability of predicting ground settlements can be obtained. The optimized neural network parameters are: the number of hidden layers N_h = 4, the number of hidden neurons in each hidden layer N_n = 15, the epoch size E_s = 1500 and the regularization parameter λ = 0.104.

The loss value of testing set during evolution is presented in Fig. 9. As shown in Fig. 9, the loss decreases rapidly with the generation increase and reaches the minimum value after 45 generation, which demonstrates that the differential evolution algorithm is efficient for the optimization of neural network architecture and hyperparameters. The final optimized hybrid model has R^2 = 94.56% and RMSE = 4.29 mm for training data

set and R^2 = 91.23% and RMSE = 6.39 mm for testing data set. To show the advantage of the proposed hybrid model, the authors have tested shallow neural networks by setting the number of hidden layers (N_h) as 1. The optimized shallow neural network parameters are: N_n = 18, E_s = 1743 and λ = 0.0. The shallow model has R^2 = 86.47% and RMSE = 6.62mm for training data set and R^2 = 85.89% and RMSE = 7.29 mm for testing data set, which indicates that shallow neural networks has poorer performance than the deep network model. Therefore, the potential of ANN may not be fully realized by merely using shallow network.

The measured and predicted settlements using hybrid model are presented in Fig. 10. The comparison shows a good agreement between the predicted and measured settlements for both training and testing sets. Most ground settlements are within 20 mm. The prediction yields quite low error in this range. However, for large settlements, especially when over 50mm, the prediction accuracy is slightly lower. This poor prediction is expected since there are not enough sample data in this range (>50mm) for the network to learn. Moreover, noises embedded in certain data can also cause error of prediction. Fig. 11 and Fig. 12 show the predicted settlement and its error in the training set and testing set, respectively. It can be seen that the error for a majority of points is smaller than the given deviation (i.e., ± 5 mm) from measurements.

As mentioned previously, the feature extraction of soils is important for the prediction performance of the model. For a comparison purpose, we added an examination where soil category rather than soil thickness around the tunnel are considered. The newly optimized neural network parameters are: N_h = 2, N_n = 28, E_s = 1994 and λ = 0.032, which produce values of R^2 = 95.28% (RMSE = 3.92 mm) for training set and R^2 = 86.95% (RMSE = 6.95 mm) for testing set. Although the indices seem better on training set than that obtained using the model considering soil thickness,

435 they tend to be poor on testing set. This big discrepancy between the training error and
436 testing error is largely due to the fact that only considering the soil category cannot
437 provide enough information for neural network to learn.

438 **4.4 Relative contribution of the inputs**

439 During the training process, neural network learns to take more seriously the
440 valuable inputs and ignore useless ones. The influence on the weights and biases from
441 the aforementioned process can be figured out from the calculation of the neural
442 network sensitivity to inputs. Fig. 13 depicts the relative importance of the input
443 parameters to the ground settlement. The relative importance is calculated by the partial
444 derivatives method (see Eq. (15)). As shown in Fig. 13, among the shield tunneling
445 operation parameters, the most important input in this case is the cutter face pressure,
446 following with the tunneling deviation and then the total shield thrust. The face pressure
447 has the highest relative importance on the ground settlement, which is consistent with
448 the research results in literature (Kasper, et al. 2006; Wang, et al. 2016). Regarding an
449 earth pressure balance shield driven tunnel, the face pressure is usually the key
450 controlling factor that is used to balance the external ground and water pressure.

451 In addition, three most important geological conditions identified by the model are
452 the thickness of sand-soil above tunnel crown, the thickness of weathered rock above
453 tunnel crown, and the groundwater level. The height of karst cave also has a
454 considerable effect on the ground settlement. Since most of the karst caves are treated,
455 the parameter KTS does not change much, resulting in a lower relative importance.
456 However, this does not imply that the treatment of karst cave is not important.

457 Although the neural network approach can provide good predictive capacity, the
458 interpretability of this kind of model is limited when compared with common linear
459 regression (Yin et al. 2018a, b). It is difficult to properly assess the relationships
460 between parameters within the model. Hence, the authors compute and plot the partial

derivatives of ground settlement to the input parameters by using the partial derivatives method. The partial derivative plots (see Fig. 14) of the hybrid model show some intuitive tendencies of ground settlement versus input parameters at each observed point (i.e., sample data point). For example, the settlement statistically tends to be negatively related to the shield thrust, but positively related to the penetration rate. If the amount of sample dataset is sufficient, the overall tendency of ground settlement relative to each parameter would be more apparent. Consequently, those previously ambiguous relationships could be sharpened by using the partial derivatives method when applying a neural network-based model.

5 Conclusions

This study proposed a hybrid neural network model for predicting shield tunneling-induced ground settlement. The effectiveness of the proposed model were verified through a case study of shield tunneling in Guangzhou Metro Line No. 9. Based on the analysis and discussion, some conclusions can be drawn as below.

(1) Different from the previous trial-and-error method, the differential evolution algorithm was incorporated into ANN framework to determine the optimal neural network architecture and hyperparameters. This algorithm can find a way to design the neural network with the optimized performance. Additional parameters introduced by differential evolution algorithm were also easy to be set up.

(2) The proposed hybrid model was facilitated by using the ‘Adam’ algorithm. This algorithm automatically adjusted learning rate and ensured less computational time for network training. More importantly, the ‘Adam’ algorithm allowed the model to perform a large number of candidate neural networks.

(3) When applying the proposed model in the field case, geological condition and shield operation parameters were used as inputs for the model. For the geological

condition inputs, thickness of soil layer was chosen to represent soil profile and a dummy variable was proposed to represent karst treatment. It is observed that this feature extraction strategy was able to convey enough geological information for the neural network to learn. Prediction results demonstrated that the proposed hybrid model can predict the settlement well during shield tunneling in karst strata.

(4) The results of sensitivity analysis indicated that the face pressure, tunneling deviation, and total shield thrust were the three most important operation parameters affecting ground settlements. These sensitive factors identified by the model enable engineers and shield operators to reasonably manage shield operation.

Acknowledgements

The research work described herein was funded by the Research Funding of Shantou University for New Faculty Member (Grant No. NTF19024-2019), "The Pearl River Talent Recruitment Program" in 2019 for Professor Shui-Long Shen (Grant No. 2019CX01G338), Guangdong Province. These financial supports are gratefully acknowledged.

Appendix

Algorithm 1: The Adam algorithm for adapting the learning rate.

Require: Step size α (Suggested value: 0.001)

Require: Small constant δ used for numerical stabilization. (Suggested value: 10^{-8})

Require: Exponential decay rates for moment estimates: ρ_1, $\rho_2 \in [0,1]$. (Suggested values: 0.9 and 0.999 respectively)

Require: Initial parameters $\boldsymbol{\theta}$. /* $\boldsymbol{\theta} = \boldsymbol{\theta}(\boldsymbol{w},\boldsymbol{b})$, $\boldsymbol{w}$ ~ weights; $\boldsymbol{b}$ ~ biases */

Require: Initialize 1st and 2nd moment vectors: $\boldsymbol{s} = \boldsymbol{0}$, $\boldsymbol{r} = \boldsymbol{0}$

Initialize time step $t = 0$

while stopping criterion not met **do**

$t \leftarrow t + 1$

Get gradients: $\boldsymbol{g} \leftarrow \nabla_{\theta} L(\boldsymbol{\theta})$

Update biased first moment estimate: $\boldsymbol{s} \leftarrow \rho_1 \boldsymbol{s} + (1-\rho_1)\boldsymbol{g}$

Update biased second moment estimate: $\boldsymbol{r} \leftarrow \rho_2 \boldsymbol{r} + (1-\rho_2)\boldsymbol{g} \odot \boldsymbol{g}$

Compute bias-corrected first moment estimate: $\hat{\boldsymbol{s}} \leftarrow \boldsymbol{s} / (1-\rho_1^t)$

Compute bias-corrected second moment estimate: $\hat{\boldsymbol{r}} \leftarrow \boldsymbol{r} / (1-\rho_2^t)$

Update parameters: $\boldsymbol{\theta} \leftarrow \boldsymbol{\theta} - \alpha \hat{\boldsymbol{s}} / \sqrt{\hat{\boldsymbol{r}} + \delta}$

end while

Return θ

References

Atangana Njock, P.G., Shen, S.L., Zhou, A., and Lyu, H.M. (2020). Evaluation of soil liquefaction using AI technology incorporating a coupled ENN/t-SNE model, *Soil Dynamics and Earthquake Engineering.*, 130, 105988. https://doi.org/10.1016/j.soildyn.2019.105988.

Bouayad, D., Emeriault, F. (2017). Modeling the relationship between ground surface settlements induced by shield tunneling and the operational and geological parameters based on the hybrid PCA/ANFIS method. Tunnelling and Underground Space Technology., 68, 142-152.

Camós, C., Molins, C. (2015). 3D analytical prediction of building damage due to ground subsidence produced by tunneling. Tunnelling and Underground Space Technology., 50, 424-437.

Chai, J.C., Shen, J.S., Yuan, D.J. (2018). Mechanism of tunneling-induced cave-in of a busy road in Fukuoka city, Japan. Underground Space., 3(2), 140-149.

Chen, R.P., Zhang P., Kang X., Zhong ZQ., Liu Y., Wu H.N. (2019a). Prediction of maximum surface settlement caused by EPB shield tunneling with ANN methods. Soils and Foundations., 59, 284-295.

Chen, R.P., Zhang P., Wu H.N., Wang Z.T., Zhong Z.Q. (2019b). Prediction of shield tunneling-induced ground settlement using machine learning techniques. Frontiers of Structural and Civil Engineering., 13(6), 1363-1378.

Cui, Q.L., Wu, H.N., Shen, S.L., Xu, Y.S., Ye, G.L. (2015). Chinese karst geology and measures to prevent geohazards during shield tunnelling in karst region with caves. Natural Hazards., 77(1), 129-152.

Dimopoulos, Y., Bourret, P., Lek, S. (1995). Use of some sensitivity criteria for choosing networks with good generalization ability. Neural Processing Letters., 2(6), 1-4.

Dindarloo, S.R., Siami-Irdemoosa, E. (2015). Maximum surface settlement based classification of shallow tunnels in soft ground. Tunnelling and Underground Space Technology., 49, 320-327.

Duchi, J., Hazan, E., Singer, Y. (2011). Adaptive Subgradient Methods for Online Learning and Stochastic Optimization. Journal of Machine Learning Research.,

12(Jul), 257-269.

Elbaz, K., Shen, S.L., Tan, Y., Cheng, W.C. (2018). Investigation into performance of deep excavation in sand covered karst: A case report. Soils and foundations., 58(4), 1042-1058.

Elbaz, K., Shen, S.L., Sun, W.J., Yin, Z.Y., Zhou, A. (2020). Prediction model of shield performance during tunneling via incorporating improved Particle Swarm Optimization into ANFIS. *IEEE Access*, 8(1), 39659-39671. https://doi.org/10.1109/ACCESS.2020.2974058

Fargnoli, V., Boldini, D., Amorosi, A. (2015). Twin tunnel excavation in coarse grained soils: Observations and numerical back-predictions under free field conditions and in presence of a surface structure. Tunnelling and Underground Space Technology., 49, 454-469.

Freitag, S., Cao, B.T., Ninić, J., Meschke, G. (2017). Recurrent neural networks and proper orthogonal decomposition with interval data for real-time predictions of mechanised tunnelling processes. Computers and Structures., 207, 258-273.

Fu, J., Yang, J., Zhang, X., Klapperich, H., Abbas, S.M. (2014). Response of the ground and adjacent buildings due to tunnelling in completely weathered granitic soil. Tunnelling and Underground Space Technology., 43, 377-388.

Gao, M.Y., Zhang, N., Shen, S.L., Zhou, A. (2020). Real-time dynamic regulation of earth pressure for shield tunneling using GRU deep learning method. *IEEE Access.*, 8(1), 64310-64323. https://doi.org/10.1109/ACCESS.2020.2984515

Gevrey, M., Dimopoulos, L., Lek, S. (2003). Review and comparison of methods to study the contribution of variables in artificial neural network models. Ecological Modelling., 160(3), 249-264.

Giardina, G., Marini, A., Hendriks, M.A.N., Rots, J.G., Rizzardini, F., Giuriani, E. (2013). Experimental analysis of a masonry façade subject to tunnelling-induced settlement. Engineering Structures., 45, 234-247.

Glorot, X., Bengio, Y. (2010). Understanding the difficulty of training deep feedforward neural networks. Proc. AISTATS., 249-256.

Goodfellow, I., Bengio, Y., Courville, A., Bengio, Y. (2016). Deep learning. MIT press Cambridge.

Kasper, T., Meschke, G. (2006). On the influence of face pressure, grouting pressure and TBM design in soft ground tunnelling. Tunnelling and Underground Space Technology., 21, 160-171.

568 Kemp, S.J., Zaradic, P., Hansen, F. (2007). An approach for determining relative input
569 parameter importance and significance in artificial neural networks. Ecological
570 Modelling., 204(3-4), 326-334.
571 Kim, C.Y., Bae, G.J., Hong, S.W., Park, C.H., Moon, H.K., Shin, H.S. (2001). Neural
572 network based prediction of ground surface settlements due to tunnelling.
573 Computers and Geotechnics., 28(6-7), 517-547.
574 Kingma, D., Ba, J. (2014). Adam: A Method for Stochastic Optimization.,
575 arXiv:1412.6980 [cs.LG].
576 Liu, X.X., Shen, S.L., Xu, Y.S., Yin, Z.Y. (2018). Analytical approach for time-
577 dependent groundwater inflow into shield tunnel face in confined aquifer.
578 International Journal for Numerical and Analytical Methods in Geomechanics.,
579 42(4), 655-673.
580 Lyu, H.M., Shen, S.L., Zhou, A.N., Yang, J. (2019). Perspectives for flood risk
581 assessment and management for mega-city metro system. Tunneling and
582 Underground Space Technology., 84, 31-44.
583 Lyu, H.M., Shen, S.L., Zhou, A., Chen, K.L. (2020a). Calculation of pressure on the
584 shallow-buried twin-tunnel in layered strata. *Tunneling and Underground Space*
585 *Technology*., 103, 103465. https://doi.org/10.1016/j.tust.2020.103465
586 Lyu, H.M., Zhou, W.H., Shen, S.L., Zhou, A. (2020b). Inundation risk assessment of
587 metro system using AHP and TFN-AHP in Shenzhen. *Sustainable Cities and*
588 *Society*, 56, 102103. https://doi.org/10.1016/j.scs.2020.102103.
589 Mair, R.J., Taylor, R.N., Burland, J.B. (1996). Prediction of ground movements and
590 assessment of risk of building damage due to bored tunneling. Geotechnical
591 Aspects of Underground Construction in Soft Ground., Balkema, Rotterdam.
592 Mair, R.J. (2008). Tunnelling and geotechnics: new horizons. Géotechnique., 58(9),
593 695-736.
594 Meschke, G. (2018). From advance exploration to real time steering of TBMs: A review
595 on pertinent research in the Collaborative Research Center “Interaction Modeling
596 in Mechanized Tunneling”. Underground Space., 3(1), 1-20.
597 Ninić, J. (2015). Computational strategies for predictions of the soil-structure
598 interaction during mechanized tunneling, Department of Civil and Environmental
599 Engineering. Ruhr-Universität Bochum, Bochum, p. 220.
600 Oña, J.D., Garrido, C. (2014). Extracting the contribution of independent variables in
601 neural network models: a new approach to handle instability. Neural Computing

602 and Applications., 25(3-4), 859-869.
603 Paliwal, M., Kumar, U.A. (2011). Assessing the contribution of variables in feed
604 forward neural network. Applied Soft Computing., 11(4), 3690-3696.
605 Peck, R.B. (1969). Deep excavations and tunneling in soft ground. 7th International
606 Conference on Soil Mechanics and Foundation Engineering, Mexico City., 225-
607 290.
608 Ren, D.J., Shen, J.S., Chai, J.C., Zhou, A.N. (2018a). Analysis of disk cutter failure in
609 shield tunnelling using 3D circular cutting theory. Engineering Failure Analysis.,
610 90, 23-35.
611 Ren, D.J., Shen, S.L., Arulrajah, A., Cheng, W.C. (2018b). Prediction model of TBM
612 disc cutter failures during tunnelling in mixed-face ground. Rock Mechanics and
613 Rock Engineering., 51(11), 3599-3611.
614 Ren, D.J., Shen, S.L., Arulrajah, A., Wu, H.N. (2018c). Evaluation of ground loss ratio
615 with moving trajectories induced in double-O-tube (DOT) tunneling. Canadian
616 Geotechnical Journal., 55(6): 894-902.
617 Ren, D.J., Xu, Y.S., Shen, J.S., Zhou, A.N. (2018d). Prediction of ground deformation
618 during pipe-jacking considering multiple factors. Applied Sciences., 8(7), 1051.
619 Sahoo, S., Russo, T.A., Elliott, J., Foster, I. (2017). Machine learning algorithms for
620 modeling groundwater level changes in agricultural regions of the U.S. Water
621 Resources Research., 53(5), 3878-3895.
622 Samui, P., Sitharam, T.G. (2008). Least-square support vector machine applied to
623 settlement of shallow foundations on cohesionless soils. International Journal for
624 Numerical and Analytical Methods in Geomechanics., 32(17), 2033-2043.
625 Santos, Jr, O.J., Celestino, T.B. (2008). Artificial neural networks analysis of São Paulo
626 subway tunnel settlement data. Tunnelling and Underground Space Technology.,
627 23, 481-491.
628 Shen, S.L., Du, Y.J., Luo, C.Y. (2010). Evaluation of the effect of rolling-correction of
629 double-o-tunnel shields via one-side loading. Canadian Geotechnical Journal.,
630 47(10), 1060-1070.
631 Shen, S.L., Cui, Q.L., Ho, C.E., Xu, Y.S. (2016). Ground response to multiple parallel
632 microtunneling operations in cemented silty clay and sand. Journal of Geotechnical
633 and Geoenvironmental Engineering., 142(5), 04016001.
634 Shen, S.L., Horpibulsuk, S., Liao, S.M., Peng, F.L. (2009). Analysis of the behavior of
635 DOT tunnel lining caused by rolling correction operation. Tunneling and

636 Underground Space Technology., 24(1), 84-95.
637 Soga, K., Laver, R.G., Li, Z.L. (2017). Long-term tunnel behavior and ground
638 movements after tunneling in clayey soils. Underground Space., 2(3), 149-167.
639 Storn, R., Price, K. (1997). Differential Evolution – A Simple and Efficient Heuristic
640 for global Optimization over Continuous Spaces. Journal of Global Optimization.,
641 11(4), 341-359.
642 Suwansawat, S., Einstein, H.H. (2006). Artificial neural networks for predicting the
643 maximum surface settlement caused by EPB shield tunneling. Tunnelling and
644 Underground Space Technology., 21, 133-150.
645 Tan, Y., Lu, Y. (2017). Why excavation of a small air shaft caused excessively large
646 displacements: forensic investigation. Journal of Performance of Constructed
647 Facilities, ASCE., 31(2): 04016083.
648 Tan, Y., Lu, Y. (2018). Responses of shallowly buried pipelines to adjacent deep
649 excavations in Shanghai soft ground. Journal of Pipeline Systems Engineering and
650 Practice, ASCE., 9(2), 05018002.
651 Tieleman, T., Hinton, G. (2012). Lecture 6.5-RMSProp, COURSERA: Neural networks
652 for machine learning. Technical Report.
653 Vorster, T., Klar, A., Soga, K., Mair, R. (2005). Estimating the effects of tunneling on
654 existing pipelines." Journal of Geotechnical and Geoenvironmental Engineering,
655 ASCE., 131(11), 1399-1410.
656 Wang, F., Lu, H., Gou, B., Han, X., Zhang, Q., Qin, Y. (2016). Modeling of shield-
657 ground interaction using an adaptive relevance vector machine. Applied
658 Mathematical Modelling., 40(9-10), 5171-5182.
659 Wongsaroj, J., Soga, K., and Mair, R.J. (2013). Tunnelling-induced consolidation
660 settlements in London Clay. Géotechnique., 63(13), 1103-1115.
661 Wu, H.N., Shen, S.L., Chen, R.P., Zhou, A., (2020). Three-dimensional numerical
662 modelling on localised leakage in segmental lining of shield tunnels. *Computers*
663 *and Geotechnics.*, 122, 103549. https://doi.org/10.1016/j.compgeo.2020.103549.
664 Wu Y.X., Lyu H.M., Han J., Shen S.L. (2019). Dewatering-induced building settlement
665 around a deep excavation in soft deposit in Tianjin, China. Journal of Geotechnical
666 and Geoenvironmental Engineering., 145(5): 05019003.
667 Wu, Y.X., Lyu, H.M., Shen, S.L., Zhou, A., (2020a). A three-dimensional fluid-solid
668 coupled numerical modeling of the barrier leakage below the excavation surface
669 due to dewatering. *Hydrogeology Journal.*, 28(4), 1449-1463.

https://doi.org/10.1007/s10040-020-02142-w.

Wu, Y.X., Shen, S.L., Lyu, H.M., Zhou, A. (2020b). Analyses of leakage effect of waterproof curtain during excavation dewatering. *Journal of Hydrology.*, 583, 124582. https://doi.org/10.1016/j.jhydrol.2020.124582.

Yin, Z.Y., Hicher, P.Y., Dano, C., Jin, Y.F. (2017). Modeling the mechanical behavior of very coarse granular materials. Journal of Engineering Mechanics., 143(1), C4016006.

Yin, Z.Y., Jin, Y.F., Shen, J.S., Hicher, P.Y. (2018a). Optimization techniques for identifying soil parameters in geotechnical engineering: comparative study and enhancement. International Journal for Numerical and Analytical Methods in Geomechanics., 42(2), 70-94.

Yin, Z.Y., Wu, Z.Y., Hicher, P.Y. (2018b). Modeling the monotonic and cyclic behavior of granular materials by an exponential constitutive function. Journal of Engineering Mechanics, ASCE., 144(4), 04018014.

Zhang, L.M., Wu, X.G., Ji, W.Y., AbouRizk, S.M. (2017). Intelligent Approach to Estimation of Tunnel-Induced Ground Settlement Using Wavelet Packet and Support Vector Machines. Journal of Computing in Civil Engineering, ASCE., 31(2), 04016053.

Zhang P. (2019). A novel feature selection method based on global sensitivity analysis with application in machine learning-based prediction model. Applied Soft Computing., 85, 105859.

Zhang P., Chen R.P., Wu H.N. (2019). Real-time Analysis and Regulation of EPB Shield Steering Using Random Forest. Automation in Construction., 106, 101860.

Zhang P., Wu H.N., Chen R.P., Chan T.H.T. (2020). Hybrid meta-heuristic and machine learning algorithms for tunneling-induced settlement prediction: A comparative study. Tunnelling and Underground Space Technology., 99, 103383.

Zhao, H.B., Yin, S. (2009). Geomechanical parameters identification by particle swarm optimization and support vector machine. Applied Mathematical Modelling., 33(10), 3997-4012.

Figure 1

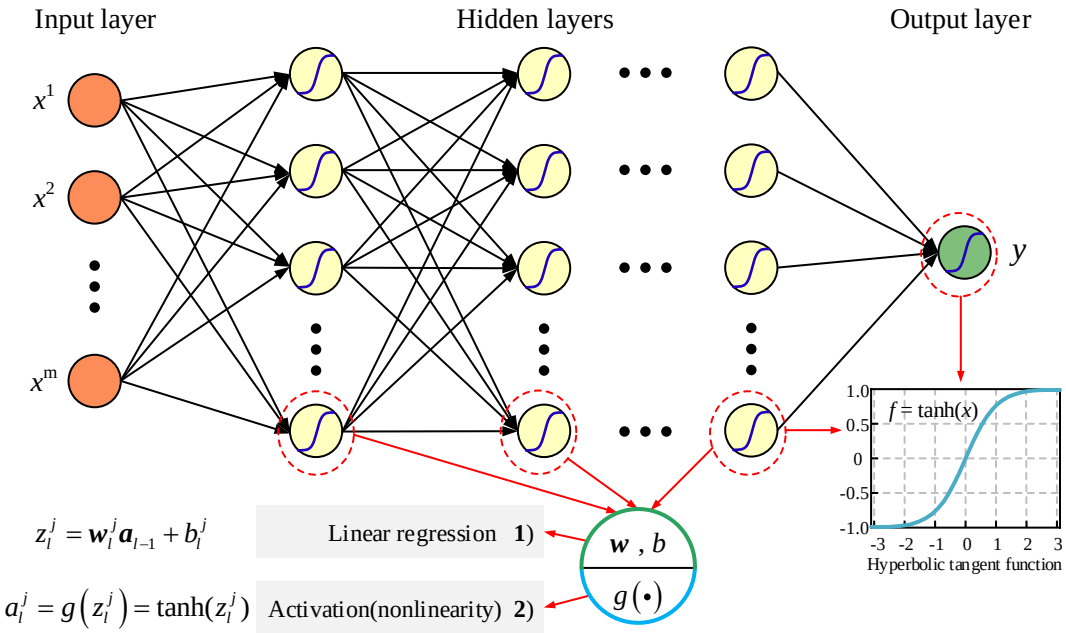

Fig. 1 Schematic diagram of artificial neural network.

Figure 2

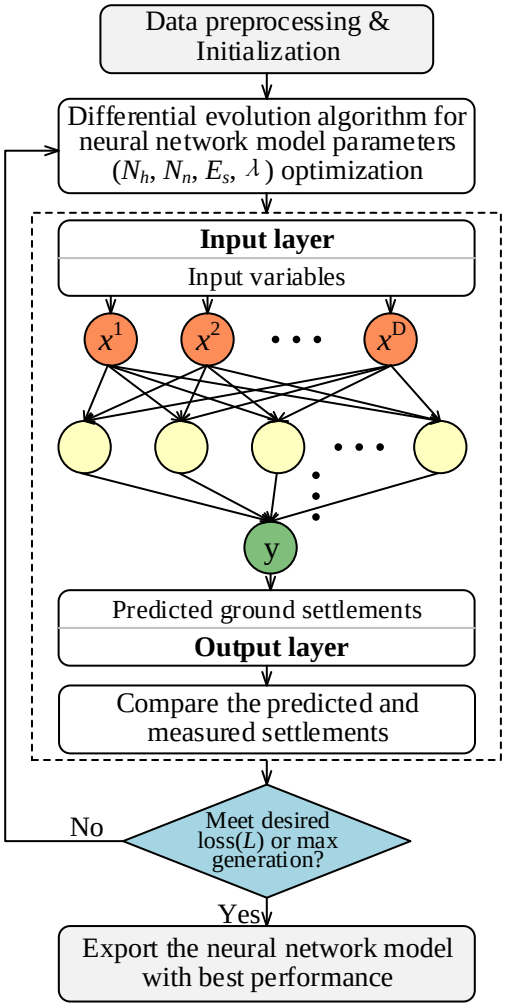

Fig. 2 Flowchart of the proposed hybrid model. The neurons in orange color represent the input variables while the green neuron represents the output variable, namely, the predicted ground settlement.

Figure 3

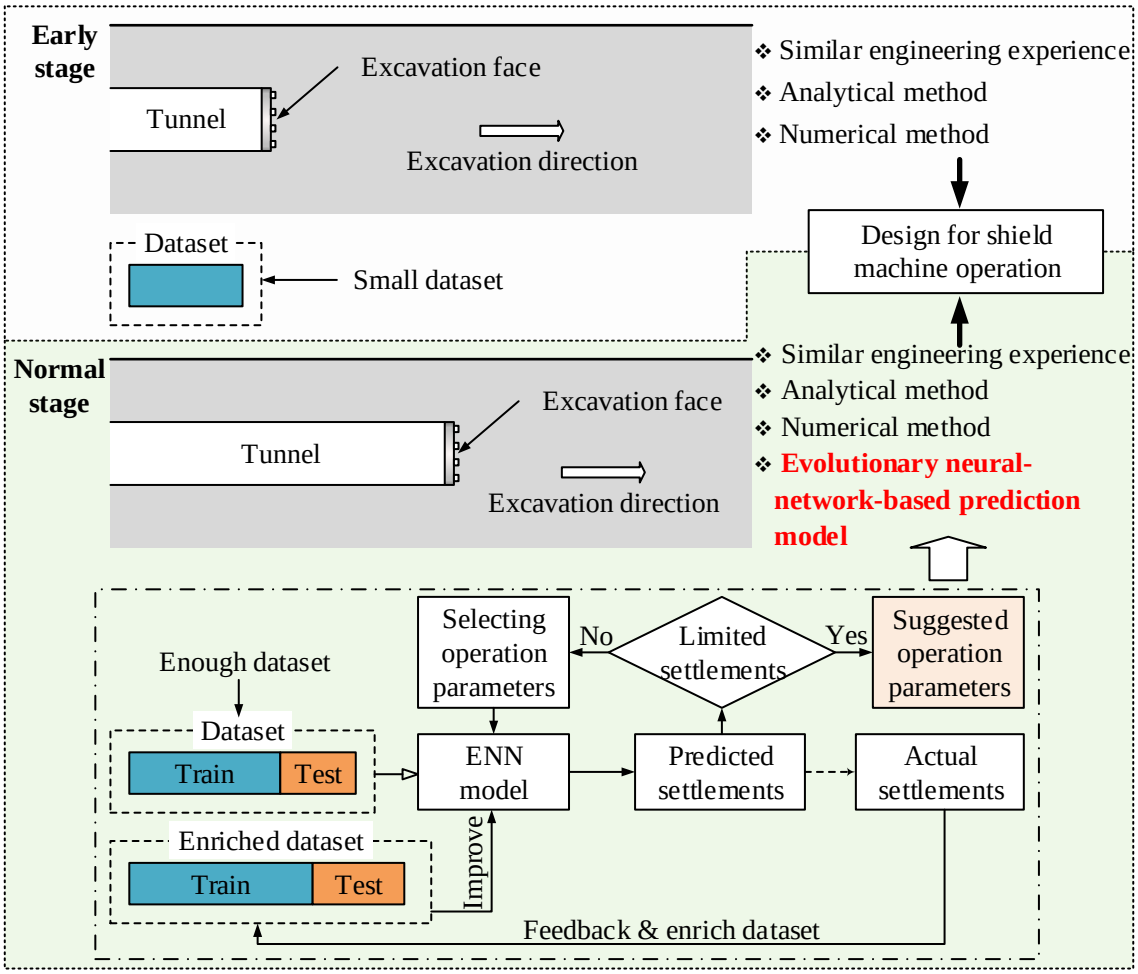

Fig. 3 Stagewise design for shield machine steering.

Figure 4

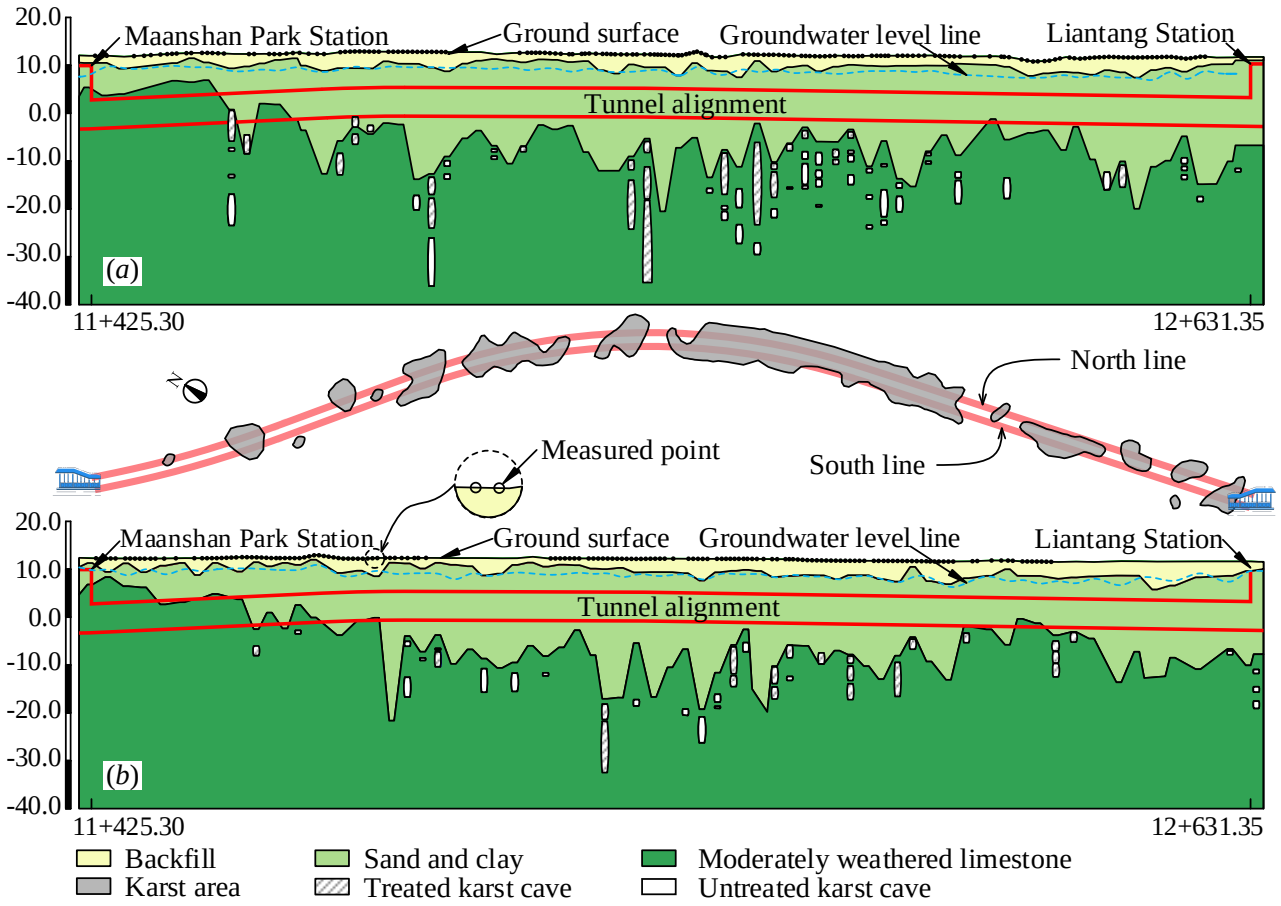

Fig. 4 Geological profile at construction site: (a) north line tunnel section; (b) south line tunnel section.

Figure 5

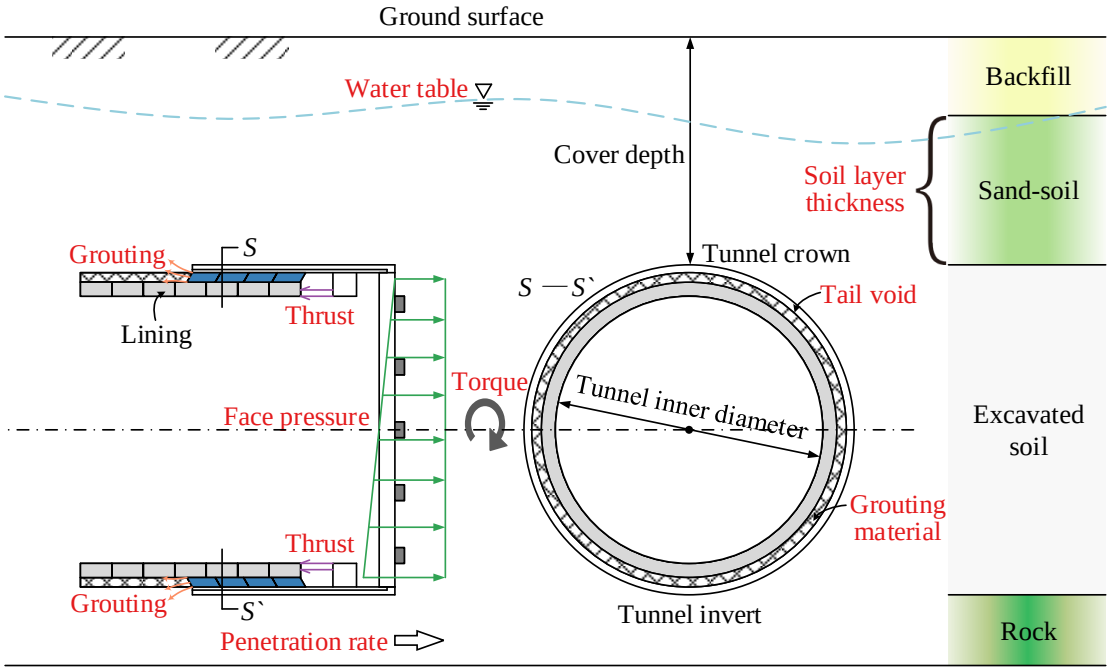

Fig. 5 Schematic illustration of geological parameters and shield operation parameters in the EPB tunneling.

Figure 6

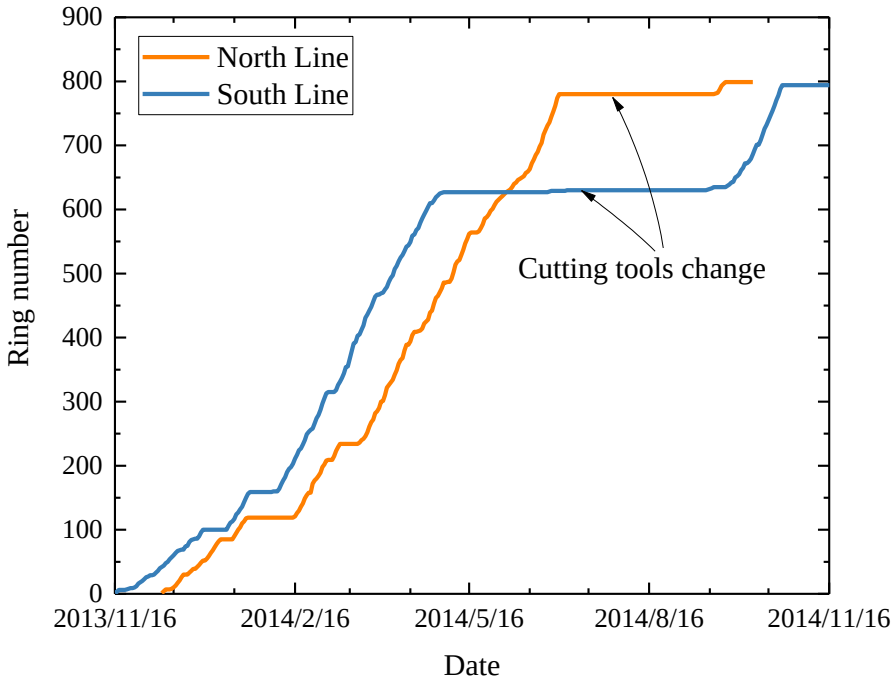

Fig. 6 Twin tunneling progress.

Figure 7

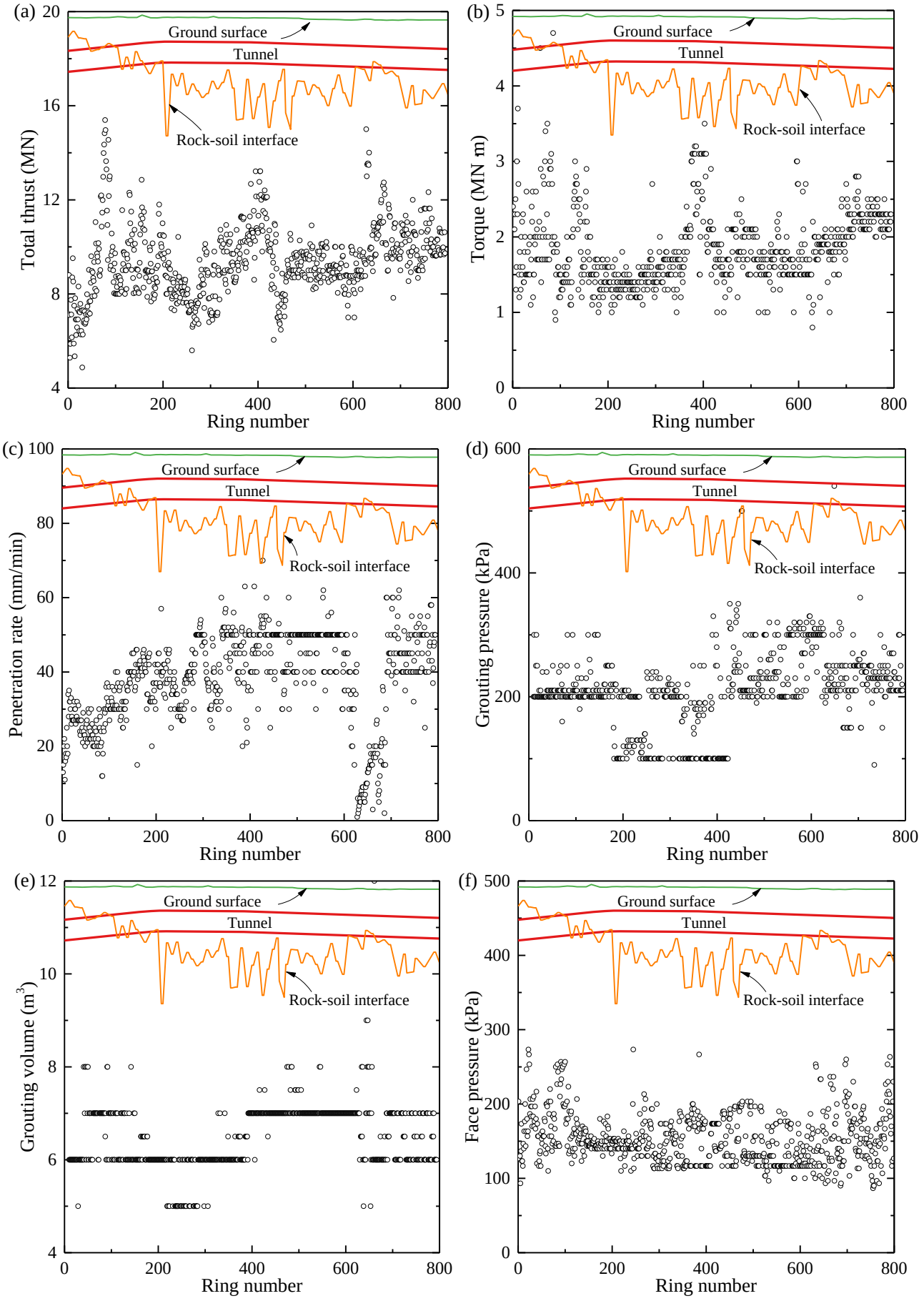

Fig. 7 Variation of shield operation parameters in tunneling process of south line. (a) total thrust; (b) cutter head torque; (c) penetration rate; (d) grouting pressure; (e) grouting volume; (f) face pressure.

Figure 8

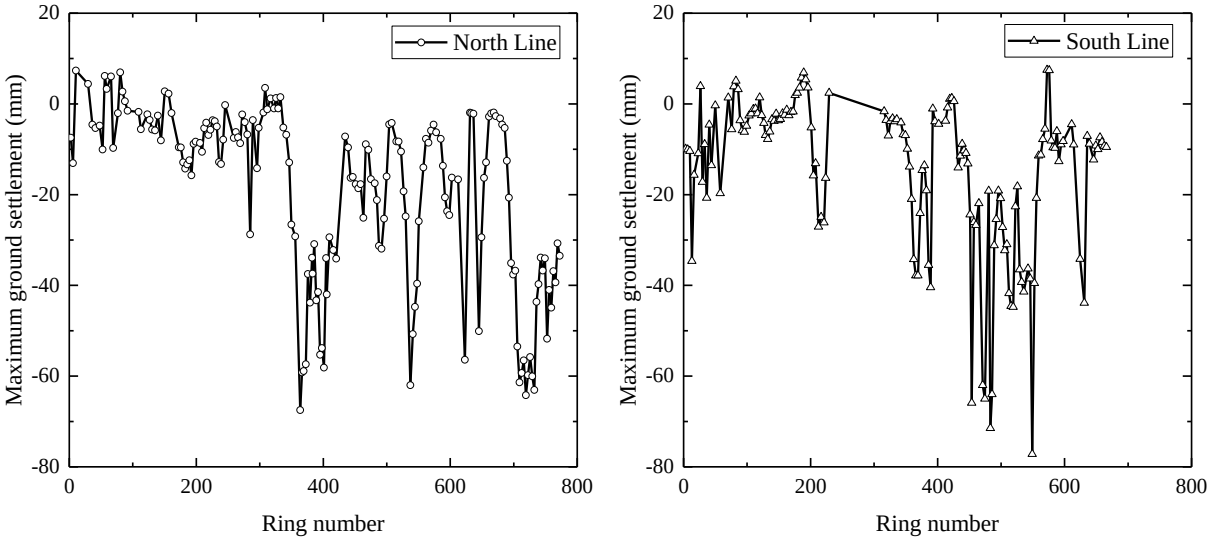

Fig. 8 Maximum ground settlement of measured points above the two tunnel centerlines.

Figure 9

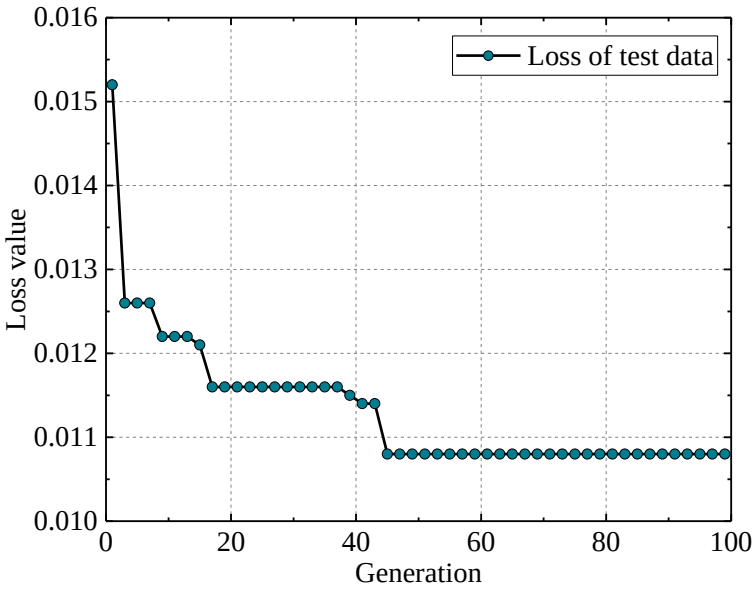

Fig. 9 Loss value of testing data set during evolution.

Figure 10

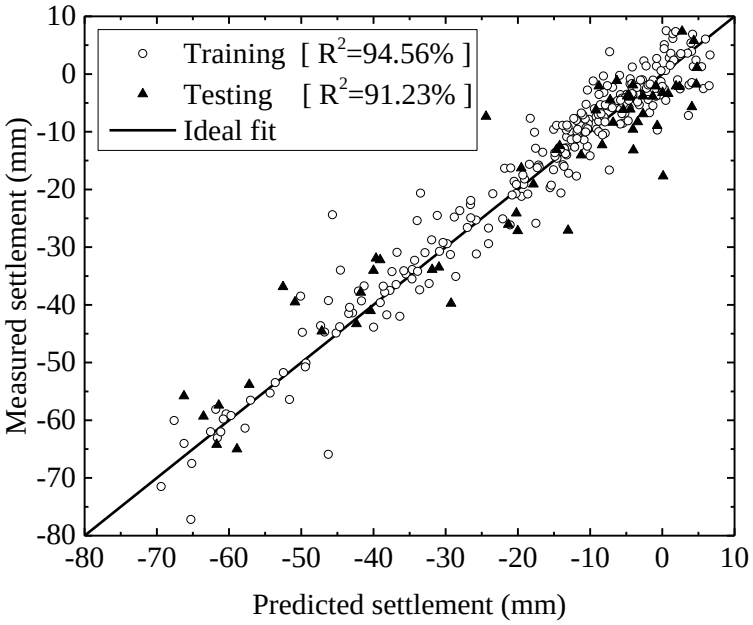

Fig. 10 Predicted vs. measured settlements for training and testing datasets.

Figure 11

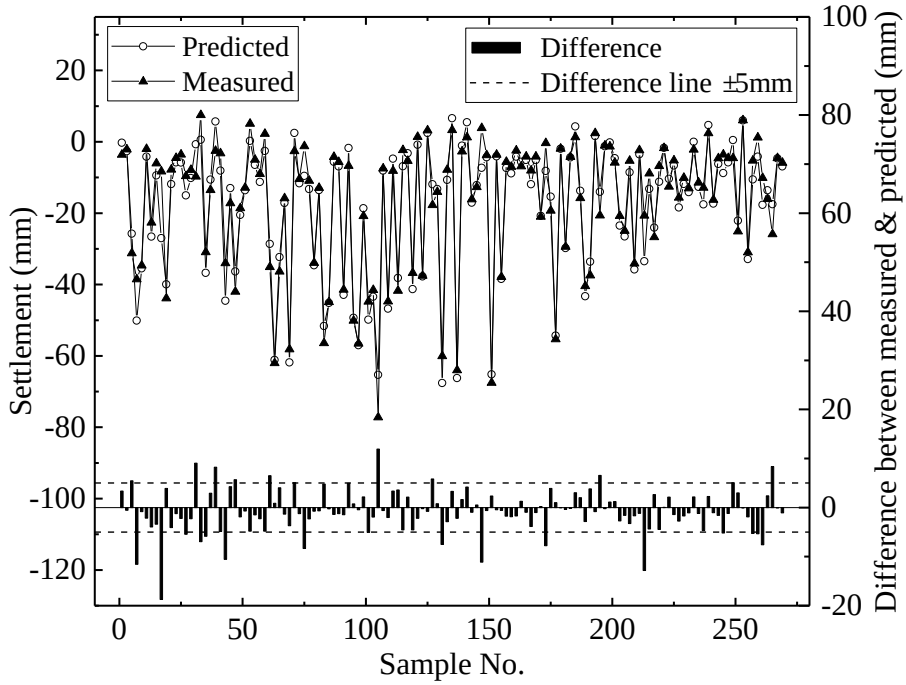

Fig. 11 Predicted settlement and its error in training set.

Figure 12

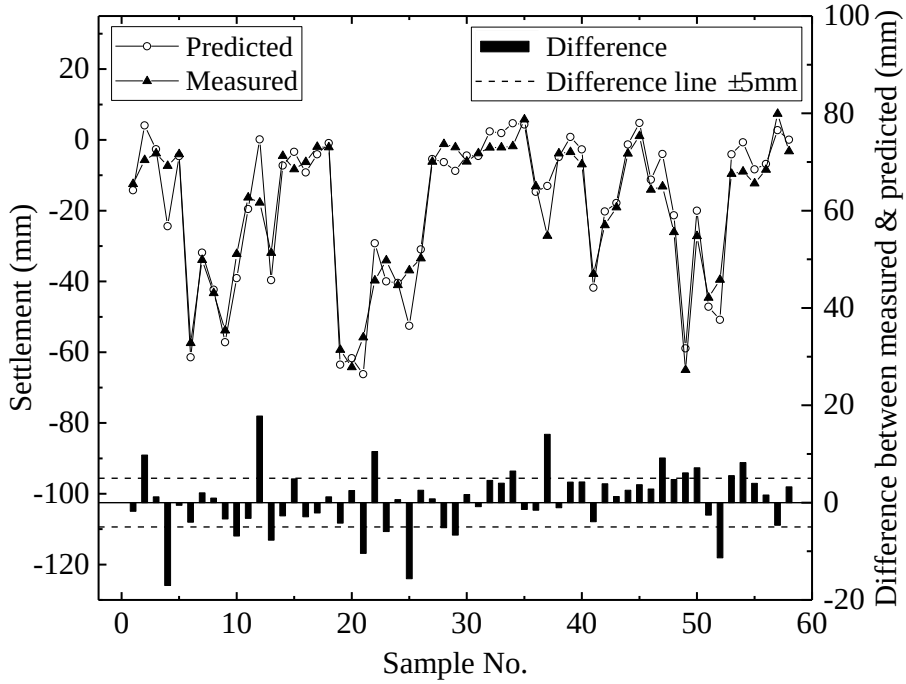

Fig. 12 Predicted settlement and its error in testing set.

Figure 13

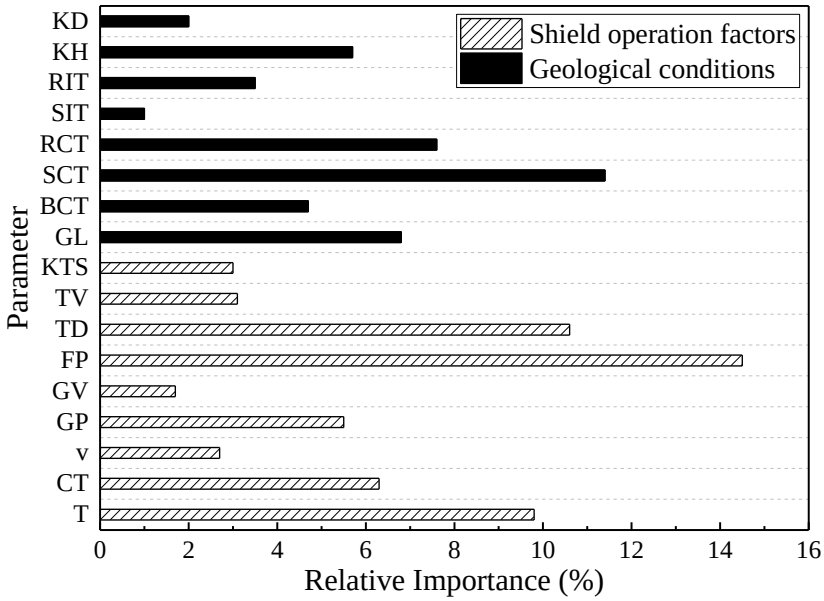

Fig. 13 Relative importance of input parameters to predicted ground settlement by partial derivatives method.

Figure 14

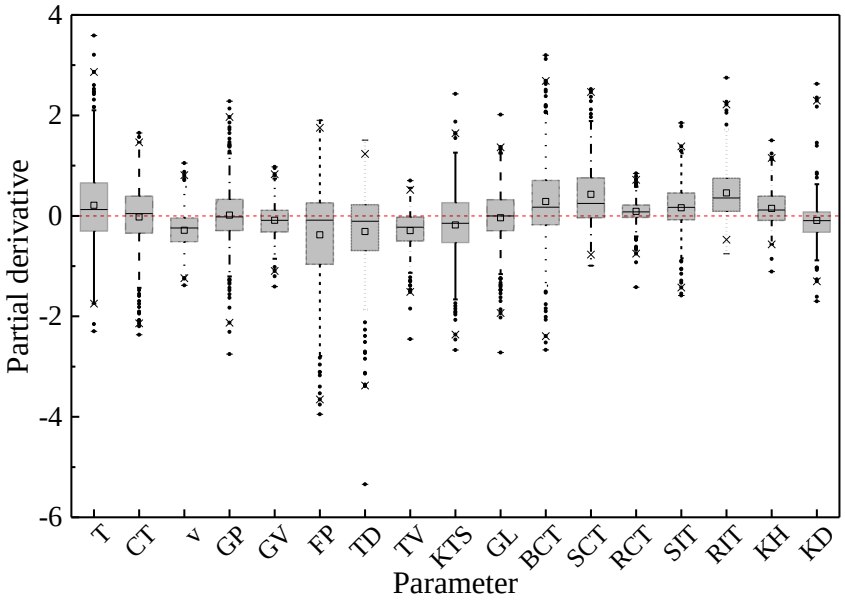

Fig. 14. Partial derivatives of ground settlement to input parameters.